7th International Building Physics Conference

IBPC2018

Proceedings

SYRACUSE, NY, USA

September 23 - 26, 2018

Healthy, Intelligent and Resilient
Buildings and Urban Environments

ibpc2018.org | #ibpc2018

Effect of Air Pressure on Moisture Transfer inside Porous Building Materials: Three-dimensional Behavior of Moisture and Air

Kazuma Fukui[1,*], Chiemi Iba[1], Shuichi Hokoi[2] and Daisuke Ogura[1]

[1]Kyoto University, Kyoto
[2]Southeast University, China

[*]*Corresponding email: be.fukui-k1820@archi.kyoto-u.ac.jp*

ABSTRACT
The effect of air pressure on moisture transfer inside porous building materials cannot be ignored in cases in which air cannot escape through the surfaces of the materials; in such cases, the air is compressed by the movement of the moisture. Therefore, in a situation in which most surfaces of a specimen are sealed or treated with surface-protecting materials (a situation that is often encountered in typical water-absorption tests), the experimental results may differ from those without sealed or treated surfaces. In the present study, the influence of air pressure on moisture transfer was investigated quantitatively.
First, the following water-absorption test was conducted. Water infiltrated into a brick through its top surface, whereas the side surfaces were sealed to prevent the transfer of moisture and air. The bottom surface was exposed to the ambient air. The water content was measured two-dimensionally during the experiment using gamma-ray attenuation. Next, to investigate how air pressure affects water infiltration, another experiment was conducted after sealing the bottom surface. The air inside the brick was expected to be compressed by the infiltrating water when the bottom surface was sealed. A water-absorption test was then performed after a small hole was made in a side surface of the bottom-sealed brick to reduce the interior air pressure. Finally, we analyzed the experiments numerically using a three-dimensional calculation model for simultaneous air and moisture transfer, assessing the validity of the model by comparing the calculated and measured water contents.
The experimental and numerical results show that water infiltration is slowed by higher air pressure inside the specimen when it is difficult for air to escape. It is also shown that the hole in the side surface helped limit the rise in air pressure to some extent.

KEYWORDS
Air pressure, Water absorption, Numerical analysis, Gamma-ray attenuation

INTRODUCTION
In water-absorption tests and measurements of water permeability, it is common to seal the side surfaces (and sometimes also the bottom surface) of the specimen to make the moisture transfer unidirectional. In addition, water-absorption tests are widely used to understand how the water-absorption rate and moisture properties are changed by surface treatments such as waterproofing and water-repellent coatings. However, because the sealed or treated surfaces may prevent the movement of not only moisture but also air, moisture infiltration may increase the air pressure in the material, thereby affecting the moisture movement.

Descamps (1997) used water-absorption tests and numerical analysis to study how air entrapment affects moisture infiltration, finding agreement between the measured and calculated sorption coefficient and inflow-surface water content. However, the moisture distribution inside the material and its temporal evolution are yet to be examined in detail. By

comparing the results of water-absorption tests on (i) a brick whose side surfaces were sealed and (ii) one whose bottom surface was also sealed, we found previously that the water absorption was clearly delayed in the latter case in which air could not escape from the brick other than through the top surface where water was absorbed (Fukui et al. 2018). In addition, we analyzed those experiments numerically using a one-dimensional model of simultaneous air and moisture transfer. However, the validity of that numerical model was not demonstrated satisfactorily because we did not consider multidirectional air flow and non-uniform distribution of air pressure in the specimen. Such effects arise from non-uniform material properties and from air bubbles appearing locally and escaping from the water-absorption surface into the water. We expect that drilling a small hole in one of the sealed surfaces would help prevent the increased air pressure from hindering moisture transfer. However, how such a hole affects the moisture transfer inside the material is also yet to be revealed quantitatively.

Therefore, in the present study, we conducted water-absorption tests on a brick to investigate how air pressure affects moisture transfer and how drilling a small hole reduces that effect. We also analyzed the experiments numerically using a three-dimensional calculation model for simultaneous air and moisture transfer, examining the accuracy of the numerical results by comparing them with the experimental ones.

WATER-ABSORPTION TESTS

Specimens and method

We conducted three experiments (see Fig. 1) on a rectangular brick of size 210 mm × 100 mm × 60 mm. In the first experiment, the side surfaces were sealed (case 1). The brick was then dried and the experiment was repeated but with the 210 mm × 100 mm bottom surface now also sealed (case 2). Finally, the brick was dried again and a 10-mm-deep hole was made in one of the 100 mm × 60 mm side surfaces of the brick with a 3-mm-diameter drill (case 3). During each experiment, water was absorbed through the top surface.

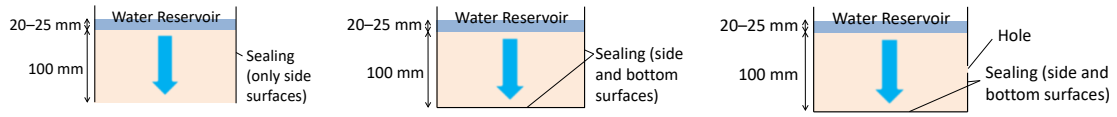

Figure 1. Schematic specimen cross sections for cases 1 (left), 2 (center), and 3 (right).

In the water-absorption tests, we used gamma-ray attenuation to measure the distribution of water content. Following Nielsen (1972), we determine the volumetric water content from the fraction of gamma rays absorbed as they pass through the brick:

$$\psi_w = -\frac{1}{\mu_{mw}\rho_w d}\ln\left(\frac{I_w}{I}\right), \tag{1}$$

where ψ_w is the volumetric water content [m^3/m^3], d is the specimen thickness [m], I_w is the gamma-ray intensity after passing through the wet specimen [cps], and μ_{mw} and ρ_w are the mass attenuation coefficient [m^2/kg] and the density [kg/m^3] of liquid water, respectively. I is the gamma-ray intensity after passing through the absolutely dry specimen [cps]. However, because the value of ψ_w is very low for an air-dried brick, instead of I we use the gamma-ray intensity after passing through the specimen in equilibrium with the ambient laboratory air. To determine I_w and I in Eq. (1), we used a measuring device whose gamma-ray source and detector could be moved vertically and horizontally on a plane normal to the direction of gamma-ray propagation (Fig. 2a). The 210 mm × 100 mm surface of the brick was irradiated

with gamma rays. At each measurement cycle, we measured the water content at 20 points (see Fig. 2b). We set the x and z axes as shown in Fig. 2b and the y axis as the direction of the gamma rays. To reduce noise, we measured for 40 s to obtain each data point. We stopped measuring from time to time to refill the water reservoir above the specimen, maintaining a water depth of 20–25 mm. We weighed the specimen before and after each experiment. We used an air conditioner to maintain the laboratory temperature at around 21°C, but we did not control the relative humidity (which fluctuated between 45% and 70%).

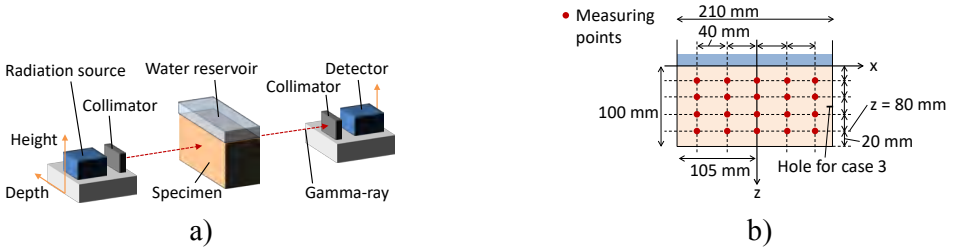

Figure 2. a) Schematic of apparatus used for gamma-ray attenuation. b) Points used to measure water content by gamma-ray attenuation.

Results and discussion

From observations made when the measurement was suspended, air bubbles appeared on the top surface of the brick and escaped into the water in case 2, whereas no such bubbles were observed in cases 1 and 3. Because air in the brick could escape through the bottom surface in case 1 and from the hole drilled in the side surface in case 3, air compressed by moisture infiltration near the top surface might have moved downward because of the air pressure gradient rather than escaping as bubbles through the top surface.

In Fig. 5, the water content measured in each experiment is shown as the data points, with the calculation results (described later) shown as the lines. Here, the results at z = 80 mm are shown as typical examples. Figure 5 shows only those data obtained during the 8 h after the start of each experiment; the water content changed little after that time. The water content clearly increases later in case 2 compared with case 1. In case 3, the water content increases at almost the same rate as in case 2, indicating that the hole did not completely prevent the rise in air pressure from hindering moisture infiltration. The results were nearly the same in cases 2 and 3 because the air bubbles (case 2) and the hole (case 3) might have suppressed the rise in air pressure inside the brick.

In each experiment, the increase in water content was slowest at x = 0 mm (i.e., the center of the brick), becoming faster nearer the side surfaces (i.e., larger absolute values of x). The sealed side surfaces and/or the horizontally non-uniform material property such as moisture diffusivity may have affected the moisture transfer. In case 3, the water content at x = 80 mm increased faster than did that at x = −80 mm. During that experiment, the air in the brick escaped from the hole, thereby lowering the air pressure at the right-hand side of the specimen. Therefore, the movement of moisture in the right half was hampered less than it was in the left half.

ANALYSIS OF SIMULTANEOUS AIR AND MOISTURE TRANSFER

In this section, we analyze case 1 numerically to estimate the moisture diffusivity of the brick. We then use that moisture diffusivity to analyze cases 2 and 3 to assess the validity of the calculation model for simultaneous air and moisture transfer.

Basic equations, calculation models, and calculation conditions

In the field of soil science, Green et al. (1970) proposed a model for air and moisture transfer and verified it using a water-absorption experiment. Referring to that model, we use the following two equations based on Darcy's law and mass conservation:

$$\frac{\partial \rho_a \psi_a}{\partial t} = \nabla \left\{ \frac{k_a}{g} \left(\nabla P_a - \rho_a g \mathbf{n} \right) \right\}, \tag{2}$$

$$\frac{\partial \rho_w \psi_w}{\partial t} = \nabla \left\{ \lambda'_P \left(\nabla P_w - \rho_w g \mathbf{n} \right) \right\}, \tag{3}$$

where ρ is the density [kg/m^3], ψ is the volume fraction [m^3/m^3], t is time [s], k_a is the coefficient of air permeability [m/s], g is the acceleration due to gravity [m/s^2], λ'_P is the water permeability due to the water pressure gradient [kg/(m·s·Pa)], P is the pressure [Pa], **n** is the unit vector in the direction of gravity, and the suffixes a and w refer to air and water, respectively. Here, we consider the compressibility of air but neglect that of liquid water, it being very small in comparison. We use the finite-difference method in the analysis, and the basic equations are discretized by the central difference for space and the forward difference for time. The spatial differential interval is 1.67, 2, and 1 mm in the x, y, and z directions, respectively. The temporal differential interval depends on P_w: for case 1, it is 10^{-6} s for $P_w < -10^8$, 10^{-4} s for $-10^8 \le P_w < -10^6$, and 0.02 s for $P_w \ge -10^6$; for cases 2 and 3, it is 10^{-6} s for $P_w < -10^8$, 5×10^{-5} s for $-10^8 \le P_w < -10^6$, and 2.5×10^{-4} s for $P_w \ge -10^6$. Here, P_w is the water pressure relative to atmospheric pressure.

Figure 3 shows the calculation models. We used the average temperature and humidity over the previous 24 h in the laboratory as the initial conditions of the brick for each experiment (case 1: 20.9°C and 55.8%; case 2: 20.8°C and 49.1%; case 3: 20.8°C and 64.1%). In cases 2 and 3, we took the initial air pressure in the brick to be atmospheric pressure. In case 1, the bottom surface was exposed to the ambient laboratory air (the vapour pressure was in equilibrium with an average temperature of 21.0°C and humidity of 63.5% during the experiment); we set the coefficient of moisture transfer between the bottom surface and the ambient air to 1.25×10^{-8} kg/(m^2·s·Pa).

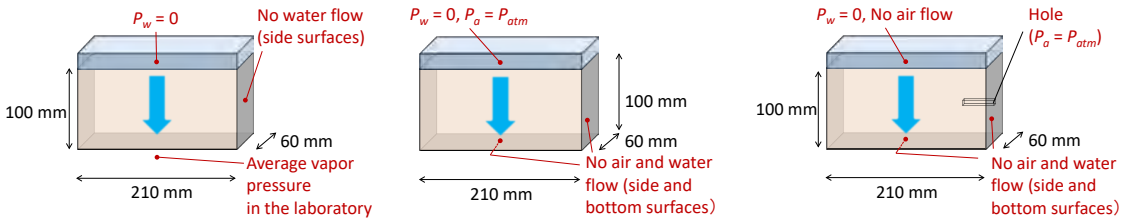

Figure 3. Calculation models for cases 1 (left), 2 (center) and 3 (right).

Because air bubbles were seen escaping from the top surface of the brick in case 2, the top surface was clearly not fully saturated with water. Therefore, in the calculation model we assumed water flow from the water reservoir to the top surface. We assumed there to be a moisture-transfer layer on the top surface of the brick, for which we used the Robin boundary condition. We set the coefficient of moisture transfer to 8.39×10^{-7} kg/(m^2·s·Pa) to ensure that the experimental and numerical results agreed in case 1. In case 2, to simplify the model, we distributed the local air loss due to the air bubbles uniformly across the top surface. Therefore,

the boundary condition for the air at the top surface was again the Robin boundary condition; the external condition was atmospheric pressure and we set the coefficient of air transfer to 4.0×10^{-10} kg/(m^2·s·Pa). In case 3, we modelled the hole as a rectangular parallelepiped that was 9.17 mm long, 3 mm high, and 2 mm wide, thereby having nearly the same surface area as the actual hole. We took the air pressure at the hole surface to be atmospheric pressure, and we neglected any flow of moisture through the hole.

Material properties used in calculation

Figure 4a shows the adsorption isotherm of the brick, which we estimated from Kumaran (1996). However, we determined ψ_w at saturation by the mass of absorbed water in case 1. According to Descamps (1997), the air permeability decreases rapidly with water content in areas of high humidity. Therefore, we took k_a to be a function of ψ_w as in Fig. 4b. Here, we took k_a in the dry state to be 2.95×10^{-9} m/s so that the experimental and numerical results agreed in case 3. Figure 4c shows the moisture diffusivity D_ψ by volumetric water-content gradient at saturation as a function of x, and Fig. 4d shows D_ψ as a function of ψ_w at x = 0, ±40, and ±80 mm. We introduced non-uniformity of D_ψ in the x direction because the calculated rate of increase of water content did not agree with the experimental results when the calculation model neglected the non-uniformity of this material property. In addition, the moisture diffusivity of a brick increases rapidly in regions of high water content (Kumaran 1996). We calculated λ'_P in Eq. (3) from D_ψ by $\lambda'_P = (D_\psi/\rho_w) \times (\partial\psi_w/\partial\mu)$, where μ is the water chemical potential for free water [J/kg]. In the analysis, we considered no other material properties to be non-uniform other than D_ψ. We did this (i) because the water content in the steady state is largely the same at all measuring points, as shown in Fig. 5, and (ii) to simplify the model.

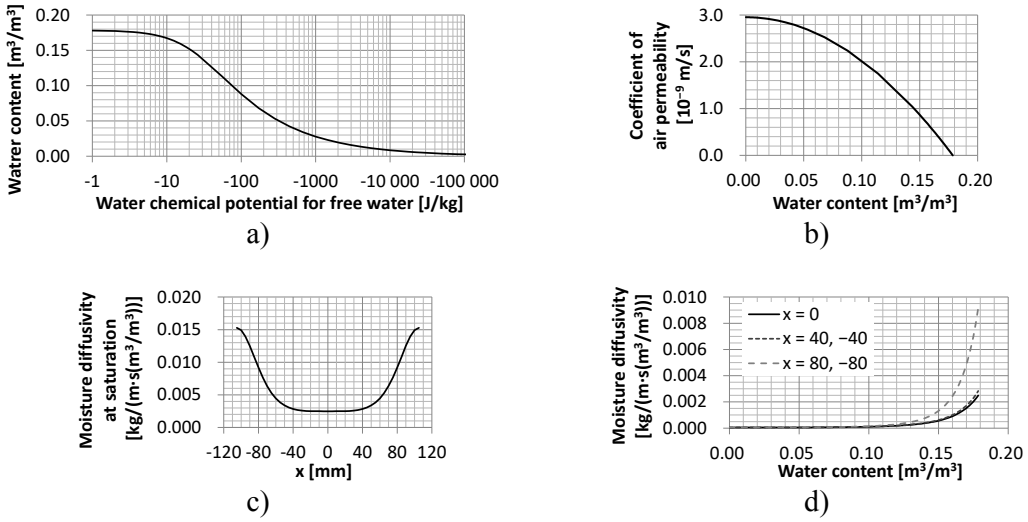

Figure 4. Material properties of the brick: a) adsorption isotherm; b) coefficient of air permeability as a function of water content; c) moisture diffusivity at saturation as a function of x; d) moisture diffusivity as a function of water content.

Calculation results and discussion

The time profiles of the calculated water content for the first 4 h are shown in Fig. 5 along with the experimental results. Because the measured water content is the average along the line of the gamma rays, we show numerical results averaged in the y direction. Because the numerical results for case 1 agree well with the experimental ones (Fig. 5a), we applied the

moisture diffusivity identified in case 1 to cases 2 and 3. In cases 2 and 3, the numerical results (Fig. 5b and c, respectively) also agree reasonably with the experimental ones except for the point at x = 0 mm, where the calculated water content rises slower than in the experiment for case 3. Calculation models that consider non-uniformity in the y and z directions may improve such agreement.

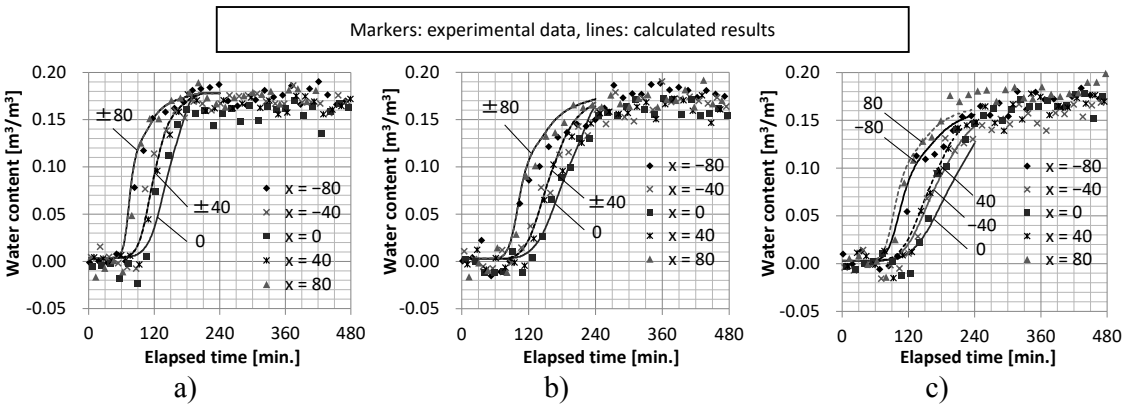

Figure 5. Calculated and measured water content for a) case 1, b) case 2, and c) case 3.

CONCLUSIONS

This study has shown that moisture infiltration in a water-absorption test is slowed considerably when air cannot escape from the specimen. It was also shown that making a small hole in the side of the specimen suppresses the rise in air pressure inside the specimen to the same extent as does air loss due to air bubbles; however, such a hole hardly changes the rate of increase of water content. Furthermore, a three-dimensional model of the simultaneous transfer of air and moisture can predict reasonably well the water content measured in the water-absorption test. Further studies of how the depth, area, and location of the small hole affect the ability of the rise in air pressure in a specimen to hinder moisture infiltration should be conducted.

ACKNOWLEDGEMENT

This research was supported by the JSPS Grant-in-Aid for Young Scientists (B) (grant no: 15K 21092; principal investigator: Chiemi Iba).

REFERENCES

Descamps F. 1997. Continuum and discrete modelling of isothermal water and air flow in porous media. *Ph.D. Thesis*, K.U. Leuven (Belgium).

Fukui K., Iba C., Hokoi S., and Ogura D. 2018. Effect of air pressure on moisture transfer inside porous building materials. *Japan Architectural Review*, https://doi.org/10.1002/2475-8876.12047.

Green D.W., Dabiri H., Weinaug C.F., and Prill R. 1970. Numerical modeling of unsaturated groundwater flow and comparison of the model to a field experiment. *Water Resources Research*, 6(3), 862-874.

Kumaran M.K. 1996. Heat, air and moisture transfer in insulated envelope parts. Final Report Volume 3 Task 3: Material Properties, International Energy Agency ANNEX24, Laboratorium Bouwfysica, K.U. Leuven (Belgium), pp. 30-36.

Nielsen A.F. 1972. Gamma-ray-attenuation used for measuring the moisture content and homogeneity of porous concrete. *Building Science*, 7(4), 257-263.